38th AIAA/ASME/SAE/ASEE Joint Propulsion Conference & Exhibit
7-10 July 2002, Indianapolis, Indiana

AIAA 2002-3778

AIAA 2002-3778
Computational Performance Estimation of Laser Ramjet Vehicle

Hiroshi Katsurayama, Kimiya Komurasaki,
and Yoshihiro Arakawa
University of Tokyo, Tokyo, Japan

38th AIAA/ASME/SAE/ASEE
Joint Propulsion Conference & Exhibit
7-10 July 2002
Indianaplis, Indiana

COMPUTATIONAL PERFORMANCE ESTIMATION OF LASER RAMJET VEHICLE

Hiroshi KATSURAYAMA*, Kimiya KOMURASAKI† and Yoshihiro ARAKAWA‡
University of Tokyo, Hongo 7-3-1, Bunkyo, Tokyo 113-8656, Japan

Abstract

The momentum coupling coefficient of a laser ramjet vehicle is calculated by CFD and an engine cycle analysis. In addition, the fraction converted to pressure and kinetic energy of a laser energy is estimated by CFD. In supersonic flights, the momentum coupling coefficient by CFD is about 1/3 of that of the engine cycle analysis mainly due to chemical frozen loss. In order to prevent the large chemical frozen loss at high altitudes, it is suggested that the laser power should be optimized according to the flight altitude.

NOMENCLATURE

A	=	cross section of a vehicle
$C.A.R.$	=	capture area ratio
C_d	=	drag coefficient
C_m	=	momentum coupling coefficient
C_p	=	specific heat at constant pressure
E	=	total energy per unit volume
E_L	=	laser energy
E_B	=	the pressure and kinetic energy converted from the laser energy
F	=	thrust
g	=	acceleration of gravity
H	=	flight altitude of the vehicle
h	=	chemical enthalpy
j	=	mass diffusion flux
M	=	Mach number
m_v	=	vehicle mass
$\dot{m}$	=	mass flow rate
P_L	=	laser power
p	=	static pressure
q	=	heat flux
R	=	gas constant
r_0	=	explosion source radius
S	=	maximum cross section of the vehicle
T	=	static temperature
t	=	time
U	=	vehicle speed
u, v	=	axial, radial velocity component
z, r, θ	=	cylindrical coordinates
γ	=	specific heat ratio
η_d	=	diffuser efficiency
η_L	=	the fractional absorption of the laser energy
η_B	=	the fraction converted to the pressure and kinetic energy of the laser energy
π_d	=	total pressure ratio
ρ	=	density
τ	=	viscous stress tensor

subscripts

i	=	inlet
s	=	species
t	=	stagnation condition
∞	=	freestream property

INTRODUCTION

In the past decade, alternatives to conventional chemical rocket launch system have been sought in order to reduce the launch cost. Especially, there are strong demand to frequently deliver payloads to a space station at a low cost. A pulsed-laser powered ramjet vehicle will be able to satisfy this demand: Since energy is provided from a laser base in ground or space to the vehicle and the atmospheric air is used as a propellant, the payload ratio is improved drastically. In addition, once a laser base is constructed, the cost is only electricity charges.

Myrabo et al. proposed an air-breathing pulsed-laser vehicle, so-called "Lightcraft," and conducted flight tests with a scaled model.[1] Their latest model, with additional solid ablative propellants, recorded the launch altitude of 121-meters.[2]

The Lightcraft consists of a nosecone forebody, a parabolic afterbody, and a cowl, as shown in Fig.1. When a high-power pulsed laser beam is focused by the afterbody mirror, air-breakdown occurs at the ring focus on the cowl. The front of produced plasma absorbs the following part of laser pulse and expands in the form of Laser Supported Detonation wave (LSD).[3] This expansion induces a blast wave. The Lightcraft gains main thrust by the blast wave sweeping on the afterbody.

Wang et al.[4] computed the flow field in the Lightcraft featuring a closed inlet. By incorporating a detailed laser-plasma interaction model, they investigated the propagation processes of LSD waves and estimated the momentum coupling co-

*Graduate student, Department of Aeronautics and Astronautics, Student Member AIAA
†Associate Professor, Department of Advanced Energy, Member AIAA
‡Professor, Department of Aeronautics and Astronautics, Member AIAA

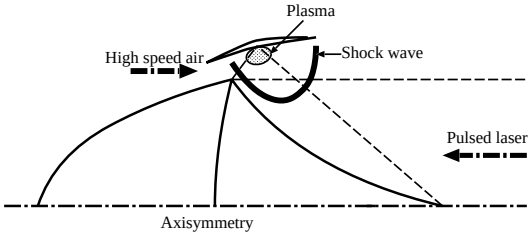

Fig.1 Pulsed-laser powered vehicle

efficient C_m, which is the ratio of cumulative impulse to one pulse laser energy.

In the present paper, C_m of a pulsed-laser ramjet vehicle is estimated by an engine cycle analysis and by CFD. Then, estimated C_m by these two methods are compared.

CFD METHOD

Governing equations

Axisymmetric Navier-Stokes equaitions are solved. Chemical reactions are treated as finite rate reactions. The following 11 species of air plasma are considered: N_2, O_2, NO, N, O, N_2^+, O_2^+, NO^+, N^+, O^+ and e^-. The effects of thermal non-equilibrium and radiative energy transfer are not considered. Then, the governing equations are given by

$$\frac{\partial \mathbf{U}}{\partial t}+\frac{\partial \mathbf{F}}{\partial z}+\frac{1}{r}\frac{\partial r\mathbf{G}}{\partial r}=\frac{\partial \mathbf{F_v}}{\partial z}+\frac{1}{r}\frac{\partial r\mathbf{G_v}}{\partial r}+\frac{\mathbf{H}}{r}+\mathbf{S}. \quad (1)$$

$$\mathbf{U}=\begin{bmatrix}\rho\\ \rho u\\ \rho v\\ E\\ \rho_1\\ \vdots\\ \rho_{11}\end{bmatrix},\mathbf{F}=\begin{bmatrix}\rho u\\ \rho u^2+p\\ \rho uv\\ (E+p)\,u\\ \rho_1 u\\ \vdots\\ \rho_{11} u\end{bmatrix},\mathbf{G}=\begin{bmatrix}\rho v\\ \rho uv\\ \rho v^2+p\\ (E+p)\,v\\ \rho_1 v\\ \vdots\\ \rho_{11} v\end{bmatrix},$$

$$\mathbf{F_v}=\begin{bmatrix}0\\ \tau_{zz}\\ \tau_{zr}\\ u\tau_{zz}+v\tau_{zr}+q_z\\ j_{1z}\\ \vdots\\ j_{11z}\end{bmatrix},\mathbf{G_v}=\begin{bmatrix}0\\ \tau_{zr}\\ \tau_{rr}\\ u\tau_{zr}+v\tau_{rr}+q_r\\ j_{1r}\\ \vdots\\ j_{11r}\end{bmatrix},$$

$$\mathbf{H}=\begin{bmatrix}0\\ 0\\ p-\tau_{\theta\theta}\\ 0\\ 0\\ \vdots\\ 0\end{bmatrix},\mathbf{S}=\begin{bmatrix}0\\ 0\\ 0\\ 0\\ \omega_1\\ \vdots\\ \omega_{11}\end{bmatrix}. \quad (2)$$

E and the equation of state are defined as

$$E = \sum_{11}\rho_s h_s(T)-p+\frac{\rho\left(u^2+v^2\right)}{2}, \quad (3)$$

$$p = \sum_{11}\rho_s R_s T. \quad (4)$$

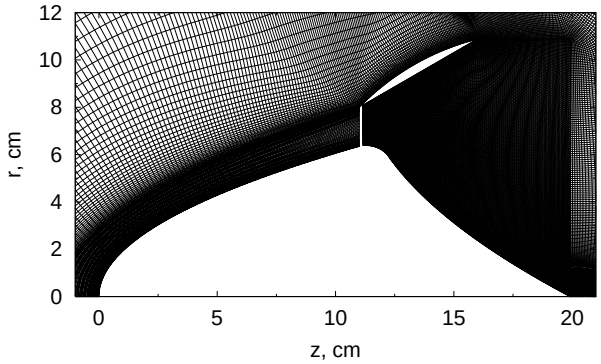

(a) Type A : 30° slope cowl (inlet is closed.)

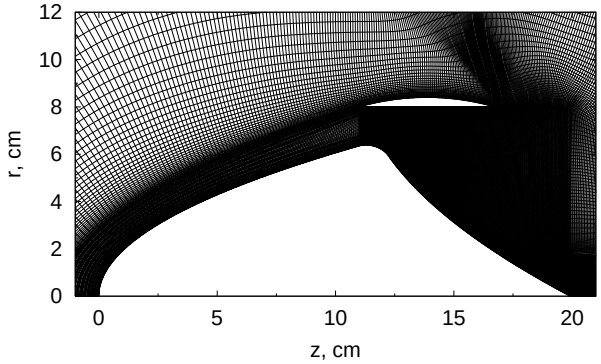

(b) Type B : non-slope cowl (inlet is open.)

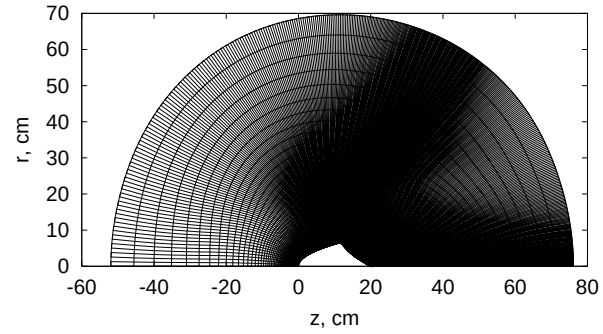

(c) Overall mesh (72,000 cells)

Fig.2 Computational meshs

h_s and the transport properties are taken from Ref.(5)

In the air chemical reaction model, the forward rates of Ref.(6) are used. The backward rates are calculated by the principle of detail balance. The chemical equilibrium constants are taken from Ref.(5).

Numerical Scheme

A cell-centered finite difference scheme is adopted. Inviscid flux is estimated with the AUSM-DV scheme[7] and space accuracy is extended to 3rd-order by the MUSCL approach with Edwards's pressure limiter.[8] Viscous flux is estimated with a standard central difference. Time integration is performed with the LU-SGS[9] scheme which is extended to 3rd-order time accuracy by

Matsuno's inner iteration method.[10] The calculation is performed with the CFL number of 2 $\sim$ 20.

Computational mesh

Figures 2 (a) $\sim$ (c) show computational meshes. The body length is set to 20 cm. The type A vehicle is almost the same as the "Label cE" Lightcraft.[1] This is used for C_m validation.

The type B vehicle with non-slope cowl is used for the calculation of a supersonic flight to reduce the aerodynamic drag.

The mesh cells are set to be fine between the cowl and body to correctly capture a blast wave. In addition, the mesh is concentrated near the wall to resolve the viscous boundary layer. The mesh width in the vicinity of the wall is $\Delta y = 80\mu$m.

The outer boundary of the computational zone is set far from the vehicle body to reduce the influence of non-physical reflection waves from the outer boundary.

Explosion source

A explosion source model[11] is employed instead of solving complex propagation processes of LSD wave: The explosion source is modeled as a pressurized volume centered at the laser focus. The focus is located at the middle on the inner cowl surface. Since LSD processes can be considered as isometric heating,[3] the density in the source is assumed to be equal to an ambient atmosphere.

The source is assumed to be in chemical equilibrium. The chemical composition is calculated by the method of Ref.(12).

η_L is chosen as 0.6 to reproduce the experimental data in Ref.(1). In addition, the dependency of C_m on the source volume is investigated.

In supersonic flights, η_L is also assumed as 0.6.

ENGINE CYCLE ANALYSIS METHOD

At first, the vehicle is launched from the ground in a pulsejet mode. Air is taken and exhausted from the rear side of the vehicle (Fig.3). In this mode, the thrust is estimated using C_m.

$$F = C_m P_L \tag{5}$$

C_m and P_L are assumed to be 250 N/MW and 3.5MW, respectively.

When thermal choking by laser heating does not occur even if air is taken from the inlet, the flight mode is switched to a ramjet mode. The thrust is computed by an engine cycle analysis assuming Humphrey cycle[13] as indicated in Fig.(4) and Fig.(5). Chemical reactions are not considered in this analysis.

The area ratio is listed in table 1. $A_1 \sim A_4$ are identical to cross sections of the type B vehicle. $A_0/S = C.A.R.$ is assumed to be 0.6.

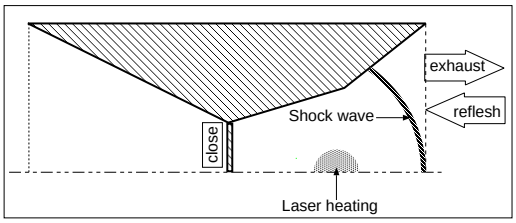

Fig.3 Schematic of pulsejet mode.

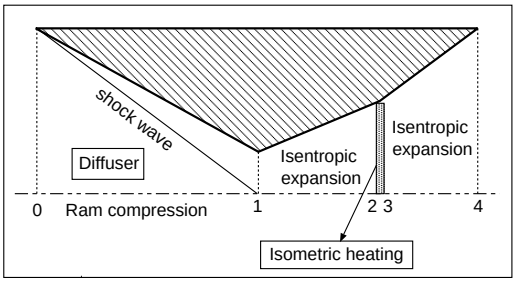

Fig.4 Ramjet engine cycle analyses.

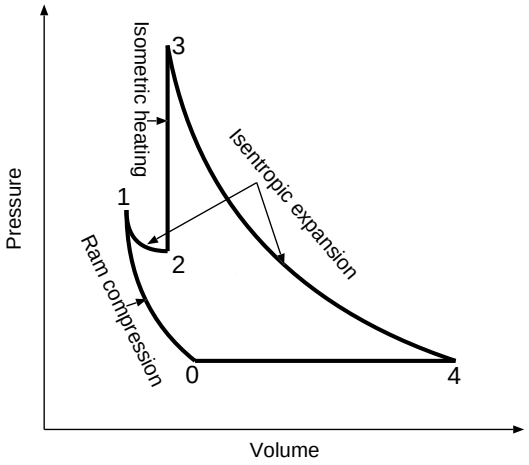

Fig.5 Humphrey cycle
(with additional isentropic expansion $1 \rightarrow 2$).

Table 1 Aera ratios of Type B vehicle.

S	A_0/S	A_1/S	$A_2/S = A_3/S$	A_4/S
201cm^2	0.6	0.38	0.75	1

Between the location 0$\rightarrow$1, air is ram-compressed. The total pressure ratio and total temperature are the following,

$$\pi_d = \frac{p_{t1}}{p_{t0}} = \left(1 + (1-\eta_d)\,\frac{\gamma-1}{2} M_0\right)^{-\frac{\gamma}{\gamma-1}} \tag{6}$$

$$T_{t1} = T_{t0}. \tag{7}$$

η_d and γ are assumed as 0.97 and 1.4, respectively.

Then, M_1 is calculated by solving the following equiation by Newton-Rapson method.

$$\frac{\left(2 + (\gamma-1)\,M_1^2\right)^{\frac{\gamma+1}{2(\gamma-1)}}}{M_1}$$

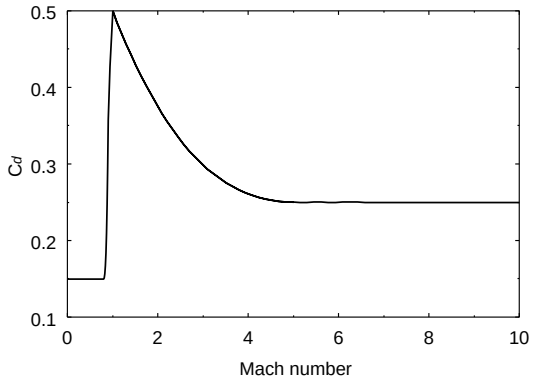

Fig.6 C_d used for the trajectory calculation.

$$= \pi_d \frac{A_1}{A_0} \frac{\left(2+(\gamma-1)\,M_0^2\right)^{\frac{\gamma+1}{2(\gamma-1)}}}{M_0}\,. \qquad (8)$$

The other phsyical properties at the location 1 are calculated by M_1, p_{t1} and T_{t1}.

Between 1→2, air is isentropically expanded to prevent thermal choking by laser heating at the throat. The physical properties at location 2 are calculated by the equations (6)∼ (8) with $\pi_d = 1$.

Between 2→3, the air is isometrically heated. A_3 is assumed to be equal to A_2. The physical properties at location 3 are calculated by mass conservation law and energy conservation law.

$$\rho_3 = \rho_2,\ u_3 = u_2,\ T_3 = T_2 + \frac{\eta_L P_{\rm laser}}{C_p \dot{m}},$$
$$p_3 = \rho_2 R T_2,\ M_3 = u_3/\sqrt{\gamma R T_3}. \qquad (9)$$

Finally, air is again isentropically expanded between the location 3→4, and the thrust is calculated as the following,

$$F = \dot{m}\,(u_4 - u_0) + A_4\,(p_4 - p_0)\,. \qquad (10)$$

The trajectory of the vehicle is calculated by solving the following motion equation by 4th order Runge-Kutta scheme.

$$m_v \frac{dU}{dt} = F - \frac{1}{2}\rho_\infty U S C_d - m_v g \qquad (11)$$

Herein, m_v is 50 g, and C_d is shown in Fig.6.

The flight condition is decided automatically by tracing the trajectory.

RESULTS AND DISCUSSION

Code validation

In order to validate the model, C_m is compared with the experimental data under the following condition: $E_L = 400$J ,$r_0 = 1.5$mm and $\eta_L = 60\%$. The estimated C_m is agreed with the experimental data, as listed in table 2.

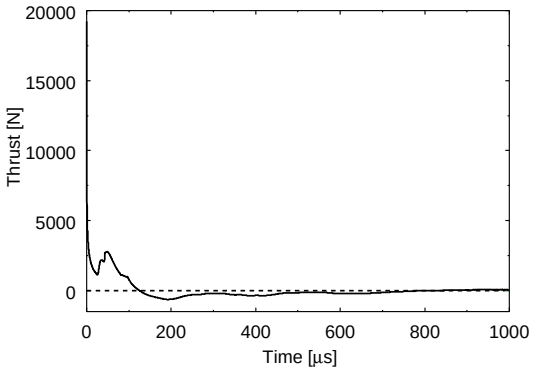

Fig.7 Thrust history ($r_0 = 1.5$mm)

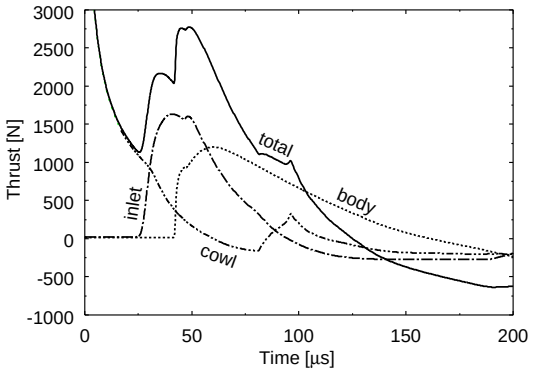

Fig.8 Each thrust received by body, cowl and closed inlet ($r_0 = 1.5$mm)

Table 2 C_m in an quiescent atmosphere.

Vehicle name	C_m (N/MW)
Label E (Myrabo[1)])	100
Type A (present)	96

The history of the axial thrust is shown in Fig.7. After the positive thrust maintains till 125 μs, the negative thrust continues till 900 μs. After 1000 μs, the thrust almost is equal to be zero.

Figure 8 shows the each thrust received by body, cowl and closed inlet till 200 μs. After the explosion source bursts at $t = 0\mu$s, the shock wave expands suddenly with weaking the intensity. Therefore, the thrust received by the cowl decreases fast.

The thrust received by the closed inlet and the afterbody decreases slower than that of the cowl.

Figures 9 (a) ∼ (c) show the propagation processes of the shock wave. The shock wave starts to sweep on the afterbody at $t = 45\mu$s. The shock wave propagates beyond the middle of the afterbody at $t = 100\mu$s. Then, the shock wave leaves the afterbody tail at $t = 190\mu$s.

Effect of r_0

In order to estimate the fraction converted to pressure and kinetic energy of the laser energy, the following efficiency is introduced.

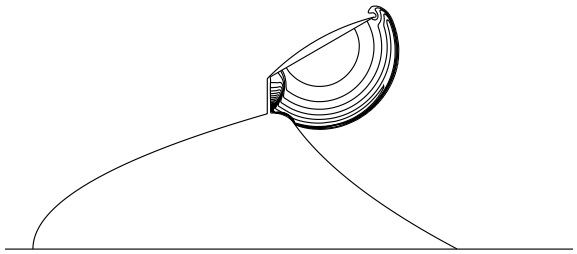

(a) At $t_1 = 45\mu$s
($p_{\max} = 5.98$atm, $p_{\min} = 0.86$atm, $dp = 0.26$atm)

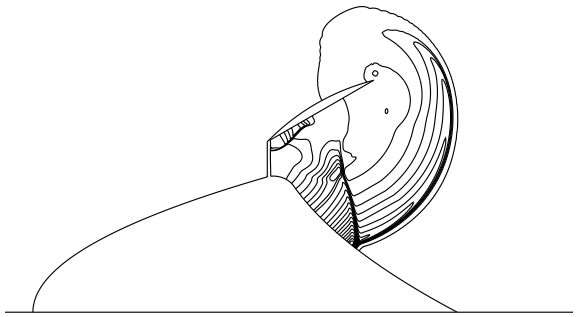

(b) At $t_2 = 100\mu$s
($p_{\max} = 3.49$atm, $p_{\min} = 0.73$atm, $dp = 0.14$atm)

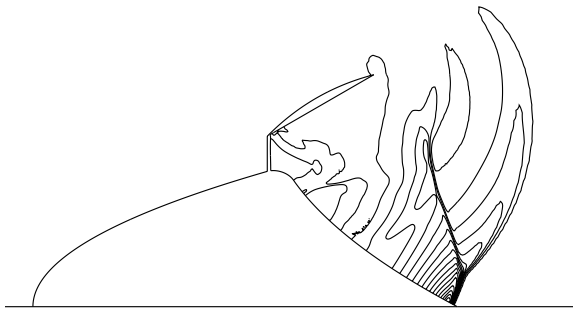

(c) At $t_3 = 190\mu$s
($p_{\max} = 3.56$atm, $p_{\min} = 0.54$atm, $dp = 0.15$atm)

Fig.9 Pressure contours in quiescent atmosphere.

$$E_B = \frac{p - p_0}{\gamma - 1} + \frac{\rho\left(u^2 + v^2\right) - \rho_0\left(u_0^2 + v_0^2\right)}{2} \quad (12)$$

$$\eta_B = \frac{\int E_B dV}{E_L}. \quad (13)$$

The subscript 0 indicates the values before the explosion. The integral is conducted over the whole computational space.

In the case of $r_0 = 1.5$mm, since the temperature in the explosion source is about 20,000K, and the ionization degree is about 25 %, large fraction of laser energy is consumed by chemical reactions in the explosion source. Table 3 shows η_B at $t = 0\mu$s, $t = 10\mu$s and $t = 100\mu$s. η_B increases by 18.8 % from $t = 0\mu$s to $t = 10\mu$s due to the energy conversion from chemical enthalpy. After $t = 10\mu$s, the rate of this energy conversion becomes slow.

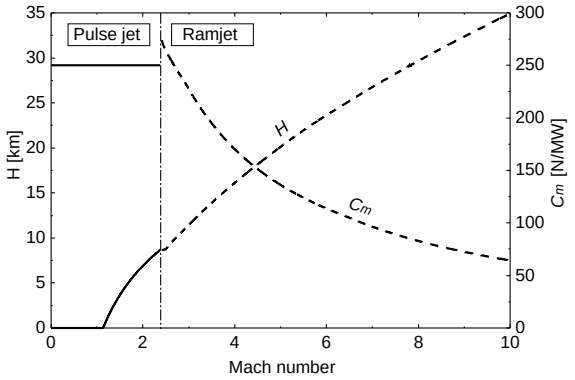

Fig.10 Mach number vs. Altitude and C_m diagram.

In the case of $r_0 = 5.5$mm, the temperature in the explosion source is about 5,000 K. Then, the energy consumed by chemical reactions is smaller than that of $r_0 = 1.5$mm. However, the difference in η_B is only 3.7 % at $t = 10\mu$s. This result shows that C_m is not so sensitive to r_0.

Table 3 η_B, %

r_0, mm	C_m	η_B (0μs)	η_B (10μs)	η_B (100μs)
1.5	96	16.1	34.9	36.2
5.5	114	29.4	38.6	40.8

Trajectory and C_m by engine cycle analysis

Figure 10 shows the Mach number vs. altitude and C_m diagram. The mode switch occurs at $M = 2.4$ and $H = 8.7$ km.

For the supersonic flow conditions for CFD, the following points are chosen from this trajectory.

Table 4 CFD simulation points of the trajectory

M	H, km	$p_\infty \times 10^{-2}$, atm	C_m, N/MW
5	20	5.5	136
8	30	1.1	83

Conditions for supersonic flights

Figures 11 (a) and (b) show the pressure contours at $M = 5$ and $H = 20$km of Type A and B vehicle. Since the oblique shock wave is generated from the tip of the cowl, the density at the focus of Type B vehicle is larger than that of Type A vehicle. Aerodynamic drag is large due to the wake generated from the body shoulder. C_d is listed in table 5. Since C_d of Type A vehicle is twice as large as that of Type B vehicle, the Type A could not produce a positive net thrust.

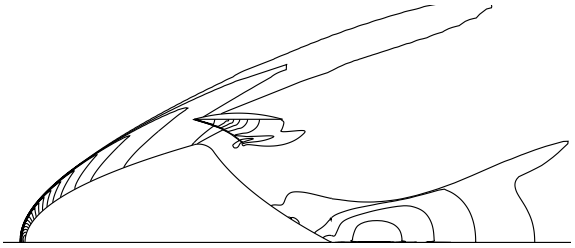

(a) Type B vehicle.
($p_{\max} = 1.8\text{atm}, p_{\min} = 6 \times 10^{-3}\text{atm}, dp = 5.1 \times 10^{-2}\text{atm}$).

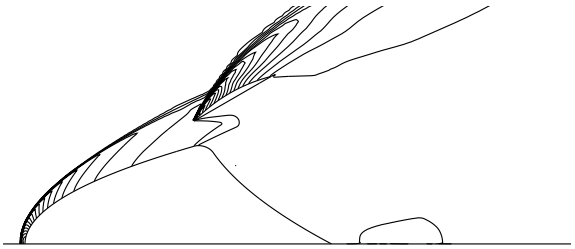

(b) Type A vehicle.
($p_{\max} = 1.8\text{atm}, p_{\min} = 2 \times 10^{-3}\text{atm}, dp = 9.0 \times 10^{-2}\text{atm}$).

Fig.11 Pressure contours of steady flow fileds at $H = 20$km and $M = 5$.

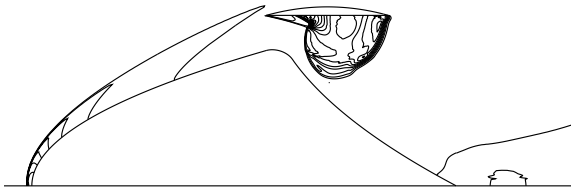

(a) At $t = 4\mu$s.
($p_{\max} = 2.57\text{atm}, \ p_{\min} = 6.1 \times 10^{-2}\text{atm}, dp = 0.13\text{atm}$)

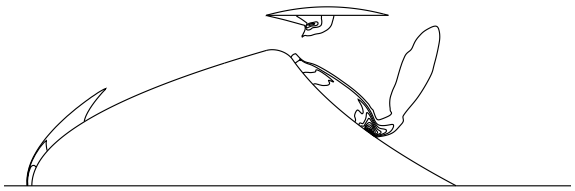

(b) At $t = 10\mu$s.
($p_{\max} = 5.36\text{atm}, \ p_{\min} = 4.1 \times 10^{-2}\text{atm}, dp = 0.27\text{atm}$)

Fig.12 Pressure contours after explosion at $H = 30$km and $M = 8$.

The $\dot{m}_i$ and C.A.R of Type B vehicle are listed in table 6. The $C.A.R.$ is defined as,

$$C.A.R. = \frac{\iint_{S_{\text{inlet}}} \rho \boldsymbol{v} \cdot \boldsymbol{ds}}{\iint_{S_\infty} \rho \boldsymbol{v} \cdot \boldsymbol{ds}} \ . \qquad (14)$$

Table 5 Aerodynamical drag.

H,km	M	C_d, N (Type B)	C_d, N (Type A)
20	5	0.26	0.53
30	8	0.25	—-

Table 6 $\dot{m}_i$ of Type B vehicle

H, km	M	$\dot{m}_i$, kg/s	$C.A.R.$, %
20	5	1.40	53.1
30	8	0.55	61.6

Explosion in Supersonic Flow field

Since C_m is not so sensitive to r_0, r_0 is decided so that the average temperature in the explosion source is about 20,000K. r_0 and the density at the focus, ρ_f, are listed in table 7

Table 7 r_0 and ρ_f in the supersonic flow.

H, km	M	$r_0$mm	$\rho_f \times 10^{-1}$kg/m^3
20	5	4.5	1.57
30	8	8.2	0.36

Figures 12 (a) and (b) show the pressure contours at $t = 4\mu$s and $t = 10\mu$s after explosion at $H = 30$km and $M = 8$. The blast wave sweeps on the afterbody without being spat out from the inlet.

Figure 13 shows the thrust histories. the thrust of $M = 8$ case is lower than that of $M = 5$ case, mainly owing to the small mass flow rate. The blast wave speed of $M = 8$ case is faster than that of $M = 5$ case because of the small ambient pressure.

Comparison of C_m calculated by CFD and engine cycle analysis

C_m by CFD and engine cycle analysis are shown in Fig.14. C_m simulated by CFD is about 1/3 of that of engine cycle analysis.

This difference would be mainly due to chemical frozen loss. Figure 15 shows η_B and $\rho_f/\rho_{(H=0\text{km})}$.

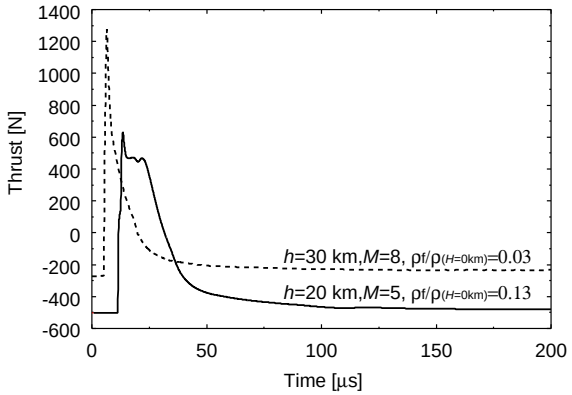

Fig.13 Thrust histories of $h = 20$km and $h = 30$km flow case.

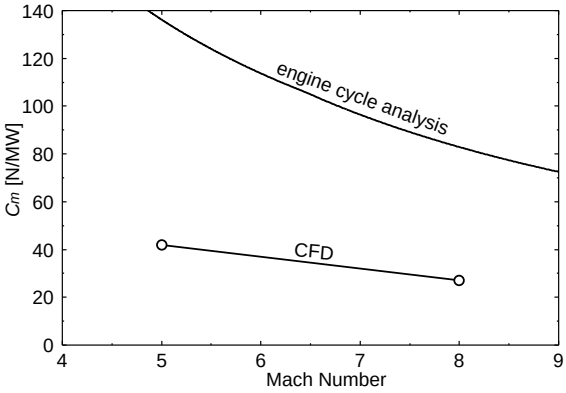

Fig.14 C_m calculated by CFD and engine cycle analysis.

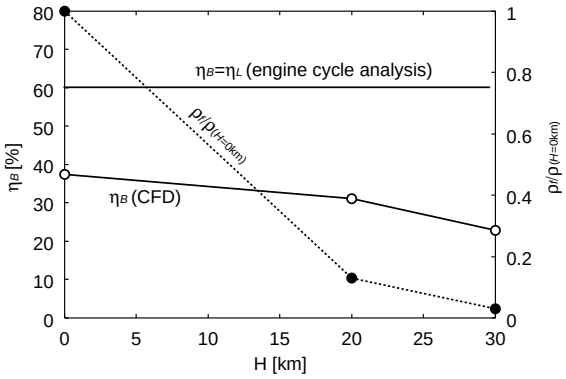

Fig.15 η_B and $\rho_f/\rho_{H=0\mathrm{km}}$

η_B of the engine cycle analysis is equal to be $\eta_L = 60\%$, because chemical reactions are not considered. However, η_B estimated by CFD is smaller than 40% due to chemical frozen loss. In addition, since the chemical frozen loss increases with decreasing ρ_f, the η_B decreases with the flight altitude.

SUMMARY

C_m of the laser ramjet vehicle is calculated by CFD and the engine cycle analysis. By the CFD code validation, C_m is found to be not so sensitive to the explosion source radius.

In supersonic flights, C_m by CFD is about 1/3 of that of the engine cycle anaylsis mainly due to chemical frozen loss. However, if the effect of chemical reactions is incorporated to the engine cycle analysis, the analysis would be able to predict the trajectory of the laser ramjet vehicle.

In addition, in order to prevent the large chemical frozen loss at high altitudes, the temperature increase near the focus needs to be suppressed. Consequently, the laser power should be optimized according to the flight altitude.

REFERENCES

(1) Myrabo, L.N., Messitt, D.G., and Mead, F.B.Jr.: Ground and Flight Tests of a Laser Propelled Vehicle, AIAA Paper 98-1001, 1998.

(2) Myrabo, L.N.: World Record Flights of Beam-Riding Rocket Lightcraft: Demonstration of "Disruptive" Propulsion Technology Flight Tests of a Laser Propelled Vehicle, AIAA Paper 01-3798, 2001.

(3) Raizer, Y.P.: Laser-Induced Discharge Phenomena, Studies in Soviet Sience, Consultants Bureau, New York and London, 1977.

(4) Wang, T.S., Mead, F.B.Jr., Larson, C.W.: Advanced Performance Modeling of Experimental Laser Lightcrafts, AIAA Paper 01-3664, 2001.

(5) Gupta, R.N., Yos, J.M., Thompson R.A. and Lee, K.P.: A Review of Reaction Rates and Thermodynamic and Transport Properties for an 11-Species Air Model for Chemical and Thermal Nonequilibrium Calculations to 30,000 K, NASA RP 1232, 1990.

(6) Park, C.: Review of Chemical-Kinetic Problems of Future Flight NASA Missions, I: Earth Entries, Calculations to 30,000 K, *J. Thermophys. Heat Transfer*, **7** (1993), pp.385-398.

(7) Wada, Y., and Liou, M.S. : A Flux Splitting Scheme with High-Resolution and Robustness for Discontinuities, NASA TM-106452, 1994.

(8) Edwards, J.R. : A Low-Diffusion Flux-Splitting Scheme for Navier-Stokes Calculations, *Computers & Fluids*, **26** (1997), pp.635-659.

(9) Jameson A., and Yoon, S. Lower-Upper Implicit Schemes with Multiple Grids for the Euler Equations, *AIAA Journal*,**25** (1987), pp.929-935.

(10) Matsuno, K. : Actual Numerical Accuracy of an Iterative Scheme for Solving Evolution Equations with Application to Boundary-Layer Flow, *Trans. Japan Soc. Aero. Space. Sci.*, **38** (1996), pp.311-322.

(11) Ritzel, D.V., and Matthews, K.: An adjustable explosion-source model for CFD blast calculations, *Proc. of 21st International Symposium on Shock Waves*, pp.97-102,1997.

(12) Botton, B., Abeele, D.V., Carbonaro, M., and Degrez G.: Thermodynamic and Transport Properties for Inductive Plasma Modeling, *J. Thermophys. Heat Transfer*, **13** (1999), pp.343-350.

(13) Bussing, T.R.A., and Pappas, G.: An Introduction to Pulse Detonation Engines, AIAA Paper 94-0263, 1994.